Two-state theory of binned photon statistics for a large class of waiting time distributions and its application to quantum dot blinking

Sándor Volkán-Kacsó

Citation: The Journal of Chemical Physics **140**, 224110 (2014); doi: 10.1063/1.4881460
View online: http://dx.doi.org/10.1063/1.4881460
View Table of Contents: http://scitation.aip.org/content/aip/journal/jcp/140/22?ver=pdfcov
Published by the AIP Publishing

Two-state theory of binned photon statistics for a large class of waiting time distributions and its application to quantum dot blinking

Sándor Volkán-Kacsó
Noyes Laboratory of Chemical Physics, California Institute of Technology, 1200 East California Boulevard, Pasadena, California 91125, USA

(Received 27 February 2014; accepted 22 May 2014; published online 12 June 2014)

A theoretical method is proposed for the calculation of the photon counting probability distribution during a bin time. Two-state fluorescence and steady excitation are assumed. A key feature is a kinetic scheme that allows for an extensive class of stochastic waiting time distribution functions, including power laws, expanded as a sum of weighted decaying exponentials. The solution is analytic in certain conditions, and an exact and simple expression is found for the integral contribution of "bright" and "dark" states. As an application for power law kinetics, theoretical results are compared with experimental intensity histograms from a number of blinking CdSe/ZnS quantum dots. The histograms are consistent with distributions of intensity states around a "bright" and a "dark" maximum. A gap of states is also revealed in the more-or-less flat inter-peak region. The slope and to some extent the flatness of the inter-peak feature are found to be sensitive to the power-law exponents. Possible models consistent with these findings are discussed, such as the combination of multiple charging and fluctuating non-radiative channels or the multiple recombination center model. A fitting of the latter to experiment provides constraints on the interaction parameter between the recombination centers. Further extensions and applications of the photon counting theory are also discussed. © *2014 AIP Publishing LLC*. [http://dx.doi.org/10.1063/1.4881460]

I. INTRODUCTION

A large class of single fluorophores subjected to steady-state excitation emit light in a stochastic manner reminiscent of an underlying telegraph-like process.[1,2] Commonly, fluorescence experiments probing such single blinking (intermittent) emitters involve binning. In this well-established technique the emitted photons are counted over short consecutive time bins resulting in a series of photon counts called an intensity trajectory. Binning may significantly influence the outcome of photon counting statistics: several blinking events may occur during a single bin, blurring the underlying states. For example, in a recent study on CdSe/CdS core/shell quantum dots (QDs) the choice of the bin time proved to be crucial for resolving what the authors called a "gray" state.[3] A fundamental limitation of the technique is that too short bin times result in excessive shot noise due to the finite number of discrete photon emissions. These Poissonian fluctuations further exacerbate the problem of determining the underlying kinetics. It is therefore of considerable interest to develop theoretical methods that explicitly take into account both binning and the discrete nature of photon emission events.

In the analysis of dichotomous-like fluorescence trajectories a more-or-less arbitrary intensity threshold is routinely defined to estimate "on" and "off" waiting time distributions (WTDs). States above the threshold are considered on and those below threshold off. Along simple exponentials, power-law WTDs are often found in single fluorophore kinetics and are ubiquitous in colloidal QDs.[4–6] Although theories for QD blinking have been proposed and later refined (see, e.g., Refs. 2 and 5, and references therein) the detailed microscopic mechanism for the power law kinetics remains unclear. Arguably, a prerequisite to the development of microscopic theory is to uncover the underlying kinetics consistent with photon counting statistics. Steady-state excitation experiments have led to an ever increasing number of discoveries, expanding the list of blinkers beyond various semiconductor nanocrystals. Power-law blinking was lately observed in various fluorophores coupled to different environments, such as perylene bisimide on Al_2O_3 surface,[7] the RC-LH1 antenna complex,[8] synthetic polymers,[9] and nitrogen vacancy centers in nanodiamonds.[10]

It was assumed that blinking in colloidal QDs follows an underlying two-state process jumping between an on and an off state.[11] This picture would naturally explain the appearance of two peaks in the intensity histogram. The finite width of these peaks would be due to the Poisson fluctuation of photon counts in the time bins. Meanwhile, the presence of inter-peak intensities would appear due to blinking dynamics within the bins. However, neither the width of the peaks, nor the inter-peak intensities were actually theoretically treated or explained so far within this picture. This important gap is filled in here by a theoretical method that takes into account the effect of binning and discrete photon counts. This allows one to also address the question of whether photon counting trajectories are consistent with the underlying two-level picture.

The present theoretical approach postulates that (1) the system has only two emission states with (2) known WTD, and (3) is characterized by renewal after each jump. For example, the two states can (and will) be assumed to follow power law WTDs. The emission states correspond to the on and off states, also termed as bright and dark states. The task is then to calculate the probability that a given number of

discrete photon emission events occur during a given bin time for steady illumination assuming properties (1)–(3). Similar assumptions were considered elsewhere, albeit not in the context of the single photon counting.[12] The present paper sheds light on the important problem of determining the number and nature of emission intensity levels in single fluorophores from a series of photon counting events. This problem was considered before via a change-point analysis,[13] which is a model-free statistical method that does not assume any prior knowledge about underlying states and kinetics.

Besides the binned intensity histogram the on and off distributions are the most important statistics extracted from trajectories. It remains unclear how the bin time and the intensity threshold affect the outcome of the analysis. The goal of this paper is to calculate the theoretical counterpart of the former, although the method can be easily extended to the latter as well. It was shown that both of these statistics can be highly biased by the two artificial quantities introduced during the analysis procedure, the bin time and intensity threshold.[14] While binned photon counting statistics have been calculated for exponential WTDs,[15] other relevant WTDs such as power laws and stretched exponentials have not yet been treated. This problem is tackled here by introducing a special kinetic scheme through which the functional form of the WTDs can be controlled.

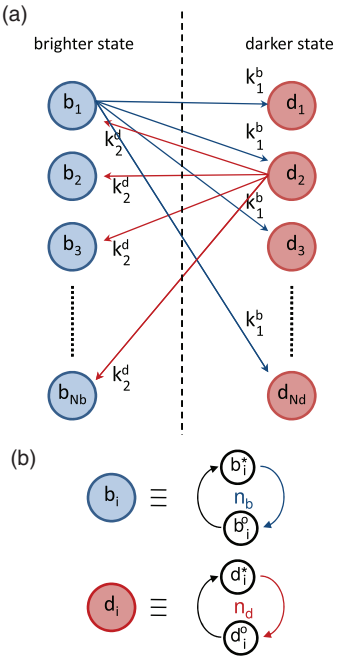

FIG. 1. (a) Reduced kinetic scheme for generating totally monotone waiting time distributions of practically arbitrary shape. The transition rates from a given bright node to all dark nodes are identical and vice-versa. Rates for only two nodes have been represented. (b) Each bright (dark) node can be further resolved into a bright (dark) fluorescent cycle with effective n_b (n_d) photon emission rates. All nodes within a manifold correspond to the same emission intensity, therefore the system produces only two intensities.

II. THEORY

A. Generic kinetic scheme and waiting time distributions

Consider the kinetic scheme in Fig. 1 governing the time evolution of single particle fluorescence. This scheme is effectively equivalent to a two-state system with WTDs that follow a weighted sum of decaying exponentials, as will be shown below. The two intensity states shall be denoted "b" and "d," suggestive of bright and dark cycles. These become on and off states for fluorophores with dark intensity below background level and bright quantum yield close to 1.

The kinetic scheme assumes a "b" and "d" manifold of states. These do not necessarily correspond to individual physical states, they are a mathematical device that allows one to control the WTD, while keeping the telegraph-like nature of the process, as will be shown below. Hence, to avoid confusion they will be simply called *nodes*. If the system is found in any of the bright (dark) manifold its fluorescence emission rate is n_b (n_d). Thus, while there could be a large number of nodes, only two intensity states result. As seen in Fig. 1(a), from any given node there is an equal rate of transitions to each node in the opposite manifold. Transition between nodes in the same manifold is forbidden. Furthermore, each node can be resolved into a fluorescent cycle (Fig. 1(b)). These excitation-relaxation cycles are identical within each manifold. They are much faster than the transitions between nodes resulting in separation of timescales.[16] Under these conditions, the time dependence of probabilities associated with the nodes follows the master equation $d\vec{P}/dt = \hat{W}\vec{P}$, where every component of $\vec{P}$ corresponds to a node. The transition matrix has a bright-dark block structure,

$$\hat{W} = \left[\begin{array}{ccc|ccc} -K_1^b & 0 & \dots & k_1^d & k_2^d & \dots \\ 0 & -K_2^b & \dots & k_1^d & k_2^d & \dots \\ \vdots & \vdots & \ddots & \vdots & \vdots & \ddots \\ \hline k_1^b & k_2^b & \dots & -K_1^d & 0 & \dots \\ k_1^b & k_2^b & \dots & 0 & -K_2^d & \dots \\ \vdots & \vdots & \ddots & \vdots & \vdots & \ddots \end{array}\right], \quad (1)$$

where $\vec{K}^b = N_d\vec{k}^b$ and $\vec{K}^d = N_b\vec{k}^d$. The condition $d\vec{P}/dt = 0$ yields the steady-state vector $\vec{P}_e$, which for the bright nodes reads

$$\left(p_e^b\right)_n = \frac{c}{k_n^b}, \quad c = \left(\sum_{n=1}^{N_b}\frac{1}{k_n^b} + \sum_{n=1}^{N_d}\frac{1}{k_n^d}\right)^{-1}. \quad (2)$$

Assuming stationary conditions the survival probability in the bright state has been shown to be[17]

$$p_b(t) = \left\langle\vec{1}, \hat{W}_{db}\exp(\hat{W}_{bb}t)\hat{W}_{bd}\vec{p}_e^d\right\rangle\left\langle\vec{1}, \hat{W}_{bd}\vec{p}_e^d\right\rangle^{-1}, \quad (3)$$

where the bracketed expression stands for the dot product operation. Simple algebra reveals that the bright WTD is a linear combination of decaying exponentials,

$$p_b(t) = \frac{1}{N_b}\sum_{i=1}^{N_b} K_i^b e^{-K_i^b t}. \quad (4)$$

Analogous expressions for the dark probabilities follow by formally interchanging b and d. Each exponential has a weight $K_i^{b(d)}$ and corresponds to a specific node.

A suitable set of nodes can reproduce practically any relevant stochastic continuous WTD, such as power laws, stretched exponentials, or a combination of exponentials. For a targeted WTD, any degree of accuracy can be reached in principle, by increasing the density (number) of nodes in waiting time. One can thus see that the present theoretical method ultimately draws on the idea of decomposing the WTD functions in a series of decaying exponentials. According to Bernstein's theorem totally monotone functions (i.e., of any order derivative also monotone) can be approximated to any degree by a weighted sum of real exponentials.[18] Efforts on decomposing functions in sums of exponentials date back to Prony (1795), with renewed interest in computational science.[19]

B. The binned photon count distribution $P(m|T)$

A generating function technique[20,21] can be employed to find the distribution of the photon number in a time interval (bin). Given the kinetic scheme in Fig. 1, a set of linear equations follow which describe the time dependence of the generating function. The knowledge of the generating function allows one to access all orders of photon counting statistics associated with monitored transitions. The components of the reduced generating function vector $\vec{f}(t,\lambda)$ obey, in block form, the equation[16]

$$\frac{d}{dt}\begin{bmatrix}\vec{f}_b\\ \vec{f}_d\end{bmatrix}=\begin{bmatrix}\hat{L}_{bb} & \hat{L}_{bd}\\ \hat{L}_{db} & \hat{L}_{dd}\end{bmatrix}\begin{bmatrix}\vec{f}_b\\ \vec{f}_d\end{bmatrix}, \tag{5}$$

where

$$\hat{L}=\begin{bmatrix}\hat{W}_{bb}-(1-\lambda)n_b\hat{1} & \hat{W}_{bd}\\ \hat{W}_{db} & \hat{W}_{dd}-(1-\lambda)n_d\hat{1}\end{bmatrix}. \tag{6}$$

Formally, the solution is

$$\vec{f}(t,\lambda)=\exp(\hat{L}t)\vec{f}(0,\lambda), \tag{7}$$

where $\vec{f}(0,\lambda)=\vec{p}_e$ is the initial condition assuming equilibrium state. The generating function is the sum of the elements of the generating function vector, which can be compactly written as

$$F(t,\lambda)=\langle\vec{1},\vec{f}(t,\lambda)\rangle=\langle\vec{1},\exp(\hat{L}t)\vec{p}_e\rangle. \tag{8}$$

Finally, calculating the quantity of interest, $P(m|T)$, the probability of a number of m counts occurring assuming a binning time T reduces to the knowledge of the generating function,

$$P(m|T)=\frac{1}{m!}\left.\frac{\partial^m F}{\partial\lambda^m}\right|_{\lambda=0}. \tag{9}$$

A Green's function technique can be employed to solve Eq. (7). The propagator (Green's function) corresponding to the equation is $\hat{F}(t,\lambda)=\exp(\hat{L}(\lambda)t)$. By formally transferring this equation to Laplace space, one finds

$$\hat{F}(s,\lambda)=(s\hat{1}-\hat{L}(\lambda))^{-1}. \tag{10}$$

One can now proceed to exchange the order of derivation with respect to λ and then apply the inverse Laplace transform. Using block-matrix representation this yields

$$P(m|T)=\frac{1}{m!}\mathcal{L}^{-1}\left\{\left\langle\left.\frac{\partial^m\hat{F}(s,\lambda)}{\partial\lambda^m}\right|_{\lambda=0}\right\rangle\right\}. \tag{11}$$

By taking advantage of the block-matrix representation it is possible to reduce $\partial_\lambda^m\hat{F}(s,\lambda)|_{\lambda=0}$ to a shape simple enough for inverting back to time domain. In most experiments the bright emission rate usually dominates over on-off switching rates and dark emission rates, therefore it is convenient to use units of n_b, resulting in formal replacements $K_n^{b(d)}/n_b\to K_n^{b(d)}$ and $k_n^{b(d)}/n_b\to k_n^{b(d)}$. Similarly, time units will be of n_b^{-1}. The ratio of dark and bright fluorescence emission rates is denoted by $r=n_d/n_b$. Note that this change of units does not affect the outcome of the calculations. Further simplifying notations are $R_b=\sum_{n=1}^{N_b}(k_n^b/A_n)$, $R_d=\sum_{n=1}^{N_d}(k_n^d/D_n)$, $S_b=\sum_{n=1}^{N_b}(1/A_n)$, and $S_d=\sum_{n=1}^{N_d}(1/D_n)$ as well as $A_n(s,\lambda)=s+1-\lambda+K_n^b$ and $D_n(s,\lambda)=s+(1-\lambda)r+K_n^d$. Using these notations one arrives to a reshaped $\hat{F}^{-1}$ matrix,

$$\hat{F}^{-1}=\left[\begin{array}{ccc|ccc}A_1(s,\lambda) & 0 & \dots & -k_1^d & -k_2^d & \dots\\ 0 & A_2(s,\lambda) & \dots & -k_1^d & -k_2^d & \dots\\ \vdots & \vdots & \ddots & \vdots & \vdots & \ddots\\ \hline -k_1^b & -k_2^b & \dots & D_1(s,\lambda) & 0 & \dots\\ -k_1^b & -k_2^b & \dots & 0 & D_2(s,\lambda) & \dots\\ \vdots & \vdots & \ddots & \vdots & \vdots & \ddots\end{array}\right]. \tag{12}$$

In block-wise notation this is equivalent to

$$\hat{F}^{-1}=\begin{bmatrix}\hat{A} & \hat{B}\\ \hat{C} & \hat{D}\end{bmatrix}. \tag{13}$$

The inversion is carried out in the block-wise manner thorough the standard formula

$$\begin{bmatrix}\hat{A} & \hat{B}\\ \hat{C} & \hat{D}\end{bmatrix}^{-1}=\begin{bmatrix}\hat{A} & \hat{0}\\ \hat{0} & \hat{0}\end{bmatrix}+\begin{bmatrix}-\hat{A}^{-1}\hat{B}\\ \hat{1}\end{bmatrix}\hat{P}^{-1}\begin{bmatrix}-\hat{C}\hat{A}^{-1} & \hat{0}\end{bmatrix}, \tag{14}$$

where $\hat{A}$ was chosen as the "pivotal" block (choosing $\hat{D}$ would lead to the same result). Thus, inverting $\hat{F}^{-1}$ effectively reduces to the inversion of the so-called Shur complement of $\hat{A}$, defined as $\hat{P}=\hat{D}-\hat{C}\hat{A}^{-1}\hat{B}$. An essential step in this calculation is to recognize that the Shur complement can be conveniently cast as

$$\hat{P}=\hat{D}-(R_b\vec{1})(\vec{k}^d)^T, \tag{15}$$

where $\hat{D}$ is diagonal, $\vec{1}$ and $\vec{k}^d=[k_1^d\quad k_2^d\quad\dots]^T$ are column vectors. A corollary of the matrix inversion (Sherman-Morison-Woodbury) lemma[22] applies to Eq. (15),

$$\hat{P}^{-1}=\hat{D}^{-1}-\frac{\hat{D}^{-1}(R_b\vec{1})(\vec{k}^d)^T\hat{D}^{-1}}{1-(\vec{k}^d)^T\hat{D}^{-1}(R_b\vec{1})}. \tag{16}$$

After carrying out the necessary algebraic steps, the blockwise components of $\langle \hat{F} \rangle$ emerge,

$$\langle \hat{F}_{bb} \rangle = \sum_{n=1}^{N_b} \frac{c}{A_n k_n^b} + c R_d \frac{1}{1 - R_b R_d} S_b^2, \tag{17}$$

$$\langle \hat{F}_{bd} \rangle = c \frac{1}{1 - R_b R_d} S_b S_d \tag{18}$$

$$= \langle \hat{F}_{db} \rangle, \tag{19}$$

$$\langle \hat{F}_{dd} \rangle = \sum_{n=1}^{N_b} \frac{c}{D_n k_n^d} + c R_b \frac{1}{1 - R_b R_d} S_d^2. \tag{20}$$

The s and λ dependence have been suppressed for simplicity. As expected, these expressions are clearly invariant with respect to the formal permutation $b \leftrightarrow d$ and $A \leftrightarrow D$.

Finding the inverse Laplace transform poses a challenge due to the $(1 - R_b R_d)^{-1}$ term. However, assuming that in experimental photon counting trajectories the emission rate is fast compared to the "typical" bright-dark switching rates, one can resort to a Taylor expansion in $R_b R_d$,

$$\frac{1}{1 - R_b R_d} = 1 + R_b R_d + 2(R_b R_d)^2 + \dots . \tag{21}$$

In practice sufficient convergence may be reached even by a first order approximation. Indeed, this is the case for power-law WTDs that are typical to colloidal CdSe/ZnS quantum dot blinking as shown in this paper.

Both s and λ dependence enter through the quantities A_n and D_n defined in the main text. Moreover, it is easy to see that

$$\left[\partial_\lambda^m A_n(s, \lambda)\right]\big|_{\lambda=0} = (-1)^m \partial_s^m A_n(s, 0), \tag{22}$$

$$\left[\partial_\lambda^m D_n(s, \lambda)\right]\big|_{\lambda=0} = (-1)^m r^m \partial_s^m D_n(s, 0). \tag{23}$$

Thus, the λ dependence is effectively removed from the calculations, and calculating the Laplace inverse is much simplified. The first terms in Eqs. (17) and (20) can be Laplace-inverted using elementary methods,[23] and yield the bright and dark Poisson peaks. Laplace-inverting the remainder of the terms is thus effectively reduced to calculating terms formally cast as

$$F'_m(l_1, l_2, l_3, l_4) = \mathcal{L}^{-1}\left\{\partial_\lambda^m (R_b^{l_1} R_d^{l_2} S_b^{l_3} S_d^{l_4})|_{\lambda=0}\right\}. \tag{24}$$

Here, $\mathcal{L}^{-1}$ stands for Laplace inversion with standard variables t and s. Finally, the main theoretical results of this paper is that the probability $P(m|T)$ of emitting m photons during a bin time T takes a simple form,

$$P(m|T) = \frac{T^m}{m!} \sum_{n=1}^{N_b} \frac{c}{k_n^b} e^{-(1+K_n^b)T} + \frac{(rT)^m}{m!} \sum_{n=1}^{N_d} \frac{c}{k_n^b} e^{-(r+K_n^d)T} + \frac{c}{m!} \sum_{q=0}^{\infty} B_q(m, T). \tag{25}$$

Here, q corresponds to the order of the $B_q(m, T)$ terms in the Taylor expansion from Eq. (21), which can be expressed as

$$B_q(m, T) = F'_m(q+1, q+1, 1, 0) + F'_m(q+1, q+1, 0, 1) + 2F'_m(q, q, 1, 1). \tag{26}$$

The first and second terms in Eq. (25) are Poissonians arising from the separate contributions of the bright and dark manifolds, with weights as a function of k_n^b and k_n^d, respectively. Assuming negligible dark emission rate ($r = 0$), given the notation $0^m = \delta_{m,0}$, the dark Poissonian narrows to a "Kronecker delta" centered at $m = 0$. This is equivalent to the true on/off-type blinking.

The third term in Eq. (25) arises from blinking dynamics producing several stochastic jumps within a bin. A method is described in Appendix A for the calculation of terms $B_q(m, T)$ of any order by the elementary Laplace inversion of $F'_m(l_1, l_2, l_3, l_4)$ terms using a numerical scheme and tensor algebra. The order of the approximation needed can be established by a simple convergence criterion, namely, that the total probability must approach one, $\sum_m P(m|T) = 1$. In practical applications where $K_n^b, K_n^d \ll n_b$ the sum often converges quickly: for QDs considered in this paper the contributions of $q > 2$ terms were negligible. The sum in Eq. (25) accounts for the photon counts in between the two Poissonians, and becomes negligible if the bin time is small compared to blinking timescales. However, for faster blinking its contribution becomes important eventually leading to a broad central feature. The central limit theorem predicts that this becomes a Gaussian for very long bin times,[24] which was verified for simple exponential WTDs ($N_b = N_d = 1$). These calculations (Appendix B) also serve to validate my method by reproducing the results of Gopich and Szabo.[16]

In practical applications one often finds that the sum in Eq. (25) already converges after the first few terms if the rates associated with each node is small compared to the bright radiative rate, i.e., $K_n^b, K_n^d \ll n_b$. In the simplest case, whereby the lowest order ($q = 0$) term yields satisfactory result, and the dark emission rate is negligible (on-off type blinking) the sum reduces to an analytic form,

$$\begin{aligned} B_0(m, T) = & \sum_{ijk} \frac{K_j^b K_k^d}{K_j^b + \epsilon_j - K_i^b} \left\{ e^{-(1+K_i^b)T} g\left[(K_i^b - K_k^d)T\right] \right. \\ & \left. - e^{-(1+K_j^b+\epsilon_j)T} g\left[(1 + K_j^b + \epsilon_j - K_k^d)T\right] \right\} \\ & + \sum_{ijk} \frac{K_j^b K_j^d}{K_k^d + \epsilon_k - K_j^d} e^{-(1+K_i^b)T} \left\{ g\left[(K_j^d - 1 - K_j^b)T\right] \right. \\ & \left. - g\left[(K_k^d + \epsilon_k - 1 - K_i^b)T\right] \right\} \\ & + 2 \sum_{ij} e^{-(1+K_i^b)T} g\left[(K_j^d - 1 - K_j^b)T\right]. \end{aligned} \tag{27}$$

In this formula the notation $g(x) = T^{m+1} {}_1F_1(1, m+1, x)/(m+1)!$ applies, where ${}_1F_1(k, l, x)$ is the confluent hypergeometric function in the standard hypergeometric series notation.[25]

III. APPLICATION TO POWER-LAW KINETICS

The present photon counting theory will be now applied to power-law kinetics. For this purpose the nodes will be chosen according to the distribution

$$K_n = \left[K_1^{\alpha-1} + A(n-1)\right]^{\frac{1}{\alpha-1}}, \quad A = \frac{K_N^{\alpha-1} - K_1^{\alpha-1}}{N-1}, \tag{28}$$

where N is the number of nodes and $n = 1, \ldots, N$. Indices b and d are implicit. Simple arguments can convince the reader that this choice of nodes leads to WTDs following an approximate inverse power law ($t^{-\alpha}$). Consider that the identity[26]

$$t^{-\alpha} = \frac{1}{\Gamma(\alpha)} \int_0^\infty K^{\alpha-2} \, (K \, e^{-Kt}) dK \tag{29}$$

can be approximated by a sum of terms $K_i e^{-K_i t}$ if K_i follow the density $\rho(K) \sim K^{\alpha-2}$. The series (28) was chosen to approximately follow this density. In the inset of Fig. 2(c) shows an example of a pair of bright and dark WTDs that were calculated by plugging two sets of nodes following Eq. (28) into Eqs. (2) and (4) and their respective dark analog. The power law dependence is limited to a range between a shortest timescale, $t_m = 1/K_N$, and a longest timescale, $t_M = 1/K_1$. The latter is a truncation time beyond which the WTD decays exponentially. Practically, the power law range can be indefinitely extended and is only limited by computational resources.

Clearly, for any given WTD there is an infinite number of choices for nodes. For example, doubling every node leaves the kinetics unaltered. Nevertheless, if the density of nodes is sufficiently large, statistical quantities depend only on the ratio of N_b/N_d and not their absolute values. One can use, for instance, the mean fluorescence quantum yield ($\langle Y \rangle$) or average photon count ($\langle n \rangle$) to set the value of this ratio. The fluorescence quantum yield is defined as the ratio of the photon emission and absorption rates. From the equation on the steady-state vectors, Eq. (2), follows that

$$\langle n \rangle = n_d \sum_{n=1}^{N_d} \frac{c}{k_n^d} + n_b \sum_{n=1}^{N_b} \frac{c}{k_n^b}, \tag{30}$$

and assuming constant absorption rate,

$$\langle Y \rangle = Y_d \sum_{n=1}^{N_d} \frac{c}{k_n^d} + Y_b \sum_{n=1}^{N_b} \frac{c}{k_n^b}, \tag{31}$$

where $Y_{b(d)}$ are the bright/dark state quantum yields. In many single fluorophore systems (such as colloidal QDs studied here[4] and dye molecules[27]), the dark state yields no measurable amount of photons ($n_d = 0$). Moreover, in high-quality QDs the bright state is assumed to have a quantum yield close to 1, therefore $\langle Y \rangle = \sum_{n=1}^{N_b} \frac{c}{k_n^b}$. It then becomes possible to estimate $\langle Y \rangle$ from trajectories and further used to set the N_b/N_d ratio when choosing an appropriate set of nodes. Therefore, once the value of the mean quantum yield is fixed by estimating it from a trajectory any theoretical quantity will only depend on the physical parameters $t_m^{b(d)}$, $t_M^{b(d)}$, and $\alpha_{b(d)}$.

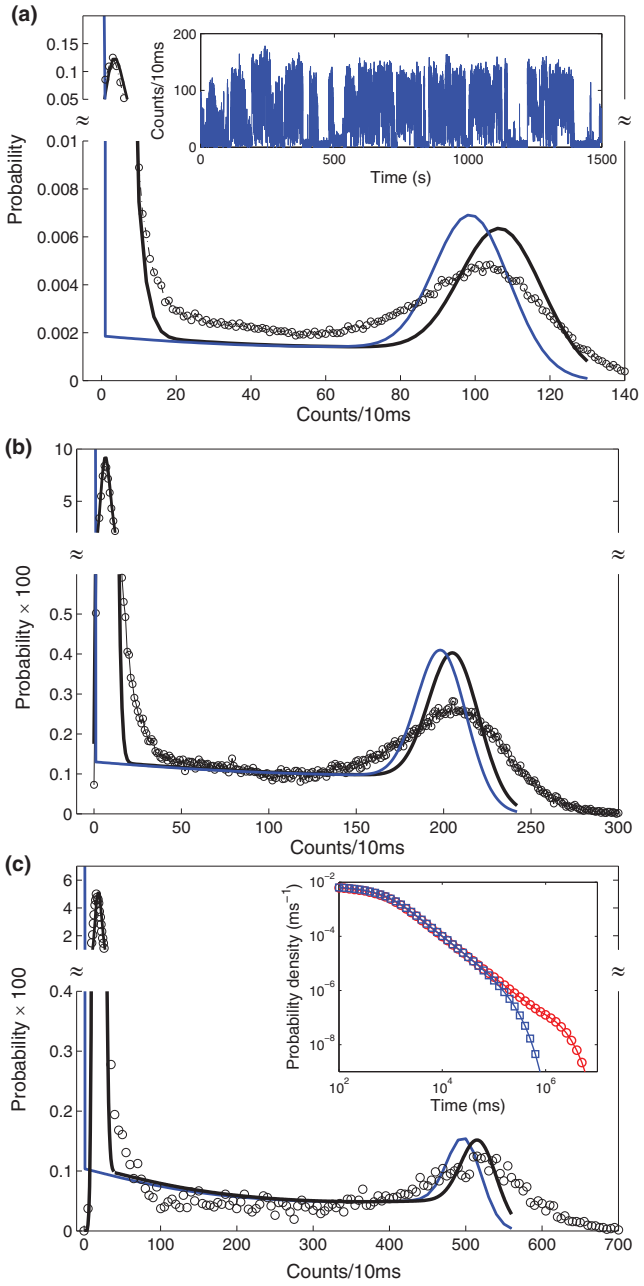

FIG. 2. Comparison of experimental and theoretical features in the intensity distribution at different bin sizes: 10 ms (a), 20 ms (b), and 50 ms (c). Normalized histograms from a single colloidal CdSe/ZnS QDs intensity trajectory are plotted (black circles) along the theoretical photon count probabilities (blue line), and their convolution to a background Poisson noise with a 4 counts/10 ms average (black line). The calculation assumed WTDs with equal shortest timescales ($t_m^{b(d)} = 2$ ms), different longest timescales ($t_M^b = 100$ ms and $t_M^d = 1$ s), and both power-law exponents $\alpha = 1.5$. The mean quantum yield was 0.1. The inset in (a) shows the experimental trajectory used in all subfigures. The inset in (c) shows the waiting time distributions (blue for on and red for off) assumed in all theoretical calculations.

IV. DISCUSSION AND COMPARISON WITH EXPERIMENT

A. Histogram features only qualitative reproduced: A "fine structure" of bright and dark states

First, the features of the histogram from a single QD trajectory will be compared with theoretical probabilities from

a qualitative perspective. This experimental trajectory (Fig. 2(a), inset) is a rather typical high-quality, stable one from a batch of 100 trajectories, and its histograms (Fig. 2, circles) clearly exhibit dichotomous blinking at various bin times. Another important feature is that between the peaks the intensity counts remain finite (non-zero) at all values, regardless of bin time. Similar trajectories from this batch have been previously analyzed elsewhere.[17,28]

The theoretical distribution in Fig. 2 (blue line) has a sharp, delta function-like peak at 0 intensity corresponding to a negligible off emission rate, $n_d \approx 0$. Its widening is simply due to an additive background Poisson noise with a mean of roughly 4 counts/10 ms. Alternatively, assuming lower noise level, the dark intensity may be higher than 0, but it is limited to 4 counts/10 ms. The bright Poissonian is centered around the average number of photons emitted in a time bin (around 100 for a 10 ms bin), assuming that the system is in that state during the whole bin time. This average corresponds to the underlying bright intensity (n_b). It is noteworthy that the fluctuations due to the discreteness of photon emission events, count corresponding to intensities significantly larger or smaller than the underlying intensity n_b would be found over long trajectories. This would apply to dark intensities as well, where (assuming $n_d > 0$) one may find bins with significantly fewer counts then the underlying intensity. Thus, the smallest and largest bin count is not a good measure of bright and dark intensity. Unbiased estimations could be subtracted by considering the peaks within the intensity histogram rather than looking at counts from individual bins.[29] For example, the dark intensity fitted to the trajectory in Fig. 2 could be anywhere in the 0–4 counts/10 ms range, depending on background noise.

According to Fig. 2, in the region between the more-or-less prominent on and off peaks, a flat feature or plateau emerges in both experimental and theoretical histograms. This feature is attributed to the blinking dynamics: due to switching times shorter than bin time, multiple bright-dark transitions occur within one bin resulting in an effective "mixing" of the two states. Furthermore, this picture remains valid if the bin times are changed (Figs. 2(a)–2(c)). Calculations assuming power law exponents $\alpha_b = \alpha_d = 1.5$ invariably yield an almost perfectly flat feature that prevails if parameters are changed, including bin time and shortest timescale for power law (Fig. 7). Meanwhile, plateaus of different height and steepness can result. The effect of binning on the inter-peak plateau may seem counter-intuitive at first glance: longer bin times result in lower-lying inter-peak plateaus. However, the combined probability of inter-peak counts in fact increases, and it is distributed among more count values, hence the lower-lying plateaus.

While the qualitative features of the histogram (Fig. 2) are roughly consistent with a two-state model, a numerical agreement is lacking. The width of the theoretical bright peak is only about half of the experimental one. The base of the dark peak is also wider in experiment. One cannot rule out a one-sided (inner side) widening of the on peaks due to the strong positive correlation between subsequent on-on durations,[30,31] neglected in this treatment. However, the widening on *both* sides of the peaks cannot be explained by correlation effects. Consequently, there must be distributions of intensity states grouped around the on (100 counts/10 ms) and off (0–4 counts/ms) maxima, rather than two single states. The persistent plateau in experimental histograms (Figs. 2(a)–2(c)) is a clear signature that the two groups do not overlap, and there is a range of intermediate intensities that the systems do not visit, an intensity state "gap." This observation validates, in the sense of a rather crude first order approximation, the two-level approach.

In calculations (Fig. 2), parameters more-or-less typical to colloidal CdSe/ZnS QD blinking were chosen, except for a rather short off correlation time. Parameters were not subtracted from an actual fit to the experimental WTDs due to their strong dependence on the choice of threshold.[14,17] The values of the shortest on and off timescales ($t_m^{b(d)}$) have not been separately determined in experiment, and they were chosen to be identical and in the millisecond range. The possibility of lower $t_m^{b(d)}$ cannot be ruled out as there is evidence that intensity fluctuations in CdSe/ZnS QDs may extend to 1/10 of a millisecond.[32] Interestingly, in a different colloidal system, the InAs QD, these fluctuations are present down to submicrosecond range.[33] Note, however, that the width of the Poisson peaks, $\sqrt{(n_{\text{background}}T)}$ (off) and $\sqrt{(n_bT)}$ (on), does not depend on the choice of the shortest or longest timescales of blinking. Therefore, changing the range of power law fluctuation would definitely not result in a quantitative agreement between the two-state theory and experiment. In the meanwhile, the present calculations (Fig. 7, Appendix D) indicate that the height of the central plateau is sensitive to the choice of the shortest blinking timescale. Thus, further investigation is warranted on utilizing this feature to reveal the shortest timescale from trajectories in systems other than CdSe/ZnS QDs, where the two-level picture rigorously applies.

The trajectory shown in Fig. 2 was chosen from a set of 100 trajectories from similar CdSe/ZnS QDs.[17,28] About half (49) of these trajectories showed two distinct peaks in their intensity histograms. Further investigation showed that qualitatively the picture of two distributions revealed in Fig. 2 trajectory applies to these as well. Nevertheless, the range of the plateaus appears to vary between trajectories which correspond to various degrees of overlap (separation) between the underlying dark and bright distribution of intensity states.

B. The inter-peak feature at different power law exponents

Practically, all stable trajectories in the analyzed batch show a rather flat inter-peak feature. The question that one might ask is whether or not the shape of this feature is sensitive to the power law exponents. Earlier theoretical studies on dichotomous processes with power law WTDs assuming continuous "monitoring" have shown that in the limit of very long bin (integration) times the inter-peak feature of the time-averaged intensity distribution displays a rich behaviour. Namely, it follows a Lamperti function, which has an approximate "U" shape for small (<1.5) power-law exponents and a "W" shape for large (>1.5) ones.[34] The former corresponds to the case of strong ergodicity breaking since the histogram does not show a peak at the ensemble average, while the latter

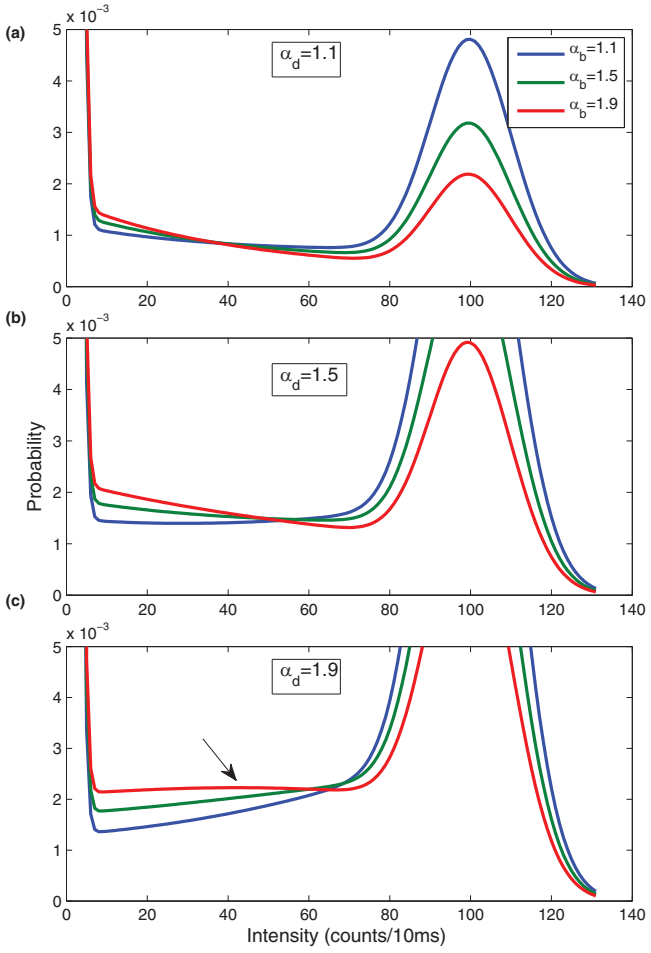

FIG. 3. Binned photon counting distributions as a function of power law exponents. The panels correspond to different off exponents: $\alpha_d = 1.1$ (a), $\alpha_d = 1.5$ (b), and $\alpha_d = 1.9$ (c). Three distributions are found within each panel, corresponding to on exponents $\alpha_b = 1.1$ (blue), $\alpha_b = 1.5$ (green), and $\alpha_b = 1.9$ (red). The other parameters were kept constant, $t_m^{b(d)} = 2$ ms, $t_M^b = 0.1$ s, $t_M^b = 1$ s, $T = 10$ ms, $n_b = 10\,\text{ms}^{-1}$, and $r = 0.01$.

corresponds to weak ergodicity breaking due to the arising of a central peak around the ensemble average.[35]

In order to investigate upon such effects for finite bin times typical for blinking experiments, the present analysis has been extended to power law exponents in the range (1.1–1.9) keeping all other parameters fixed. Figure 3 summarises the finding and reveals a behaviour somewhat reminiscent of the Lamperti function. While the Lamperti function features are much less pronounced due to the shortness of bin time, one can identify all the relevant cases. In addition, the features are broadened due to the discrete nature of photon detection events. Thus, the two-peaked distributions with a round depression found at small exponents (Fig. 3(a)) correspond to the "U" shape, while the three-peaked distribution at large exponents with a shallow intermediate peak (arrow in Fig. 3(c)) corresponds to the "W" shape. More flattened plateaus are found when at least one of the exponents is ∼1.5 which is close to the transition point from the "U" to the "W" shape.[35] Meanwhile, the inter-peak region shows various degrees of tilting both sloping towards the on and off states. The tilt is more sensitive to the power law exponent than the curvature. According to calculations in Fig. 3 the non-flat features are not very pronounced and, if exist, may be difficult to detect in histograms from trajectories due to statistical noise. Further investigation is warranted to establish whether the power law exponents could be estimated using the present theoretical framework from trajectories by comparing the flatness, tilt, and possible the height of the interpeak features. The details of such a study are deterred to a future publication.

C. Practical method for quantitative comparison with many trajectories

Next, a systematic method will be demonstrated for the comparison of theory with multiple trajectories taking advantage of certain quantities that can be calculated with simple analytic formulas. Arguably, for a deeper understanding of the physical processes involved in blinking, the proper quantitative analysis of a large set of experimental trajectories is more desirable than considering only one or a few. A comparison based on complete intensity histograms (Fig. 2) becomes impractical for large numbers of trajectories. This difficulty can be overcome by evaluating only the total contribution of either the two Poisson peaks or the central feature ($P_{bd}(T)$),

$$P_d(T) = \sum_{m=0}^{\infty} \frac{(rT)^m}{m!} \sum_{n=1}^{N_d} \frac{c}{k_n^b} e^{-(r+K_n^d)T}, \tag{32}$$

$P_b(T)$ is analogous and $P_{bd}(T)$ follows from normalization. Thus, the contributions of the three features can be calculated by simple summations. In Fig. 4, theory and experiment are compared based on P_d written as a function of the mean quantum yield [Eq. (31) and following discussion]. The

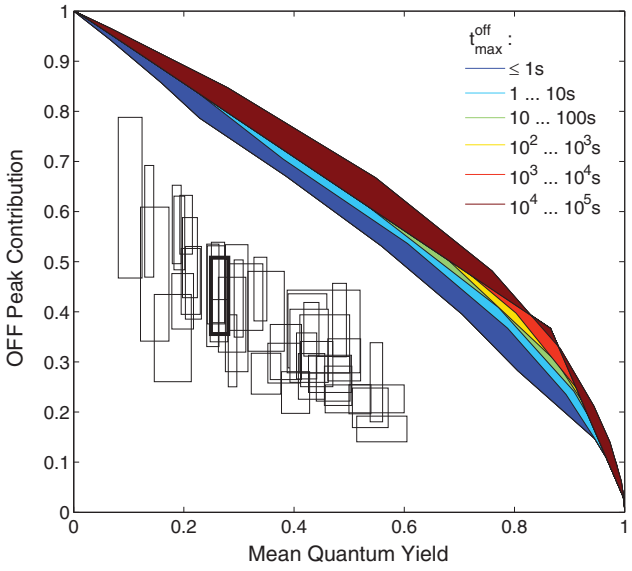

FIG. 4. Comparison of theory and experiment based on the probability associated with the dark peak in the histogram. The on-state quantum yield was assumed ∼1. Each rectangle corresponds to one telegraph-like trajectory (48 total). The thick line indicates the trajectory from Fig. 2. The rectangles enclose confidence areas that correspond to a confidence level larger than 95%. Shaded areas correspond to theory. On and off power law exponents were varied in the 1.2–1.8 range, the shortest blinking timescales in the 10 μs–1 ms range, the longest on timescales in the 100 ms–100 s range.

first few intensity points of the off peaks (bins with ~1–4 counts) were found to be approximately Poissonian in 48 out of 49 dichotomous-like trajectories (one trajectory had a wide off peak that could not be fitted by this method). The fitting of Poissonians allowed for an estimation of the experimental off probability (Appendix C). Also, the mean quantum yield and the associated confidence intervals were estimated by appropriate statistical procedures. The confidence areas show the limits within which both quantities are found with a high (>95%) probability. The shaded areas correspond to theory assuming a complete range of parameters consistent with blinking. On a more technical note, the calculation of a multitude of P_d values and the statistical analysis of a considerable set of trajectories required only modest computational power.

The longest off times are known to be extremely long,[36] probably surpassing the very length of the trajectories (1 h). However, it is not necessary to perform calculations beyond some limit. According to the comparison on Fig. 4, as one considers increasingly high values for the longest off time, the discrepancy between theory and experiment becomes more pronounced. Even unrealistically low theoretical values are found to be inconsistent with experiment. Thus, for the calculation of the probability contribution of dark peaks the difficulty arising from a possibly infinite correlation length and thus non-ergodicity[28] is effectively removed. Furthermore, experimental off power law distributions extending to infinity would result in smaller mean quantum yields if one would measure longer trajectories (aging effect). This would in fact further increase the gap between theoretical and experimental points in Fig. 4. It, therefore, becomes clear that none of the 48 dichotomous-like trajectories are consistent with the simple two-level model, nor is the 49th trajectory due to both of its wide dark and bright peaks. The remainder of the trajectories showed various instabilities, such as monotonous global trends (either increasing or decreasing) which may be attributed to the QDs slowly diffusing in and out of the focal plane. Nevertheless, if one were to assume that these trends are intrinsic to blinking rather than artifacts, these unstable trajectories would be even harder to reconcile with the two-level assumption than the dichotomous ones.

D. Implications of the distributed states on models of blinking

Elucidating the statistics associated with photon counting trajectories can help further develop and refine theories of quantum dot blinking. The present investigation has revealed information about features of the underlying intensity state distribution based on a number of such trajectories. In line with these findings, theories should allow for a quasi-continuum of states grouped around a bright and a dark maximum. They should also account for the observation that the bright and dark intensity states are separated in the intensity histograms of high-quality trajectories. This separation is indicated by the presence of an inter-peak plateau predicted by calculations in this paper. Finally, models have to take into account the rather narrow distribution of dark intensity states manifesting as a narrow (but still wider-than-Poissonian) peak in almost all of the analyzed trajectories.

While the long-held contention of a two-state picture is undoubtedly a useful approximation, for a more realistic treatment it should be further developed. The more nuanced picture that emerges is that a "fine structure" applies to both bright and dark intensity states where the wide distribution of the former poses a major challenge. Indeed, the present findings contribute to the growing body of evidence supporting a multi-state picture of blinking.[3,13,32,37–39] Emission lifetime measurements in CdSe/ZnS QDs have demonstrated that the off state can be further resolved into a manifold of states[38,39] which is consistent with the evidence indicating a distribution of dark intensity states (Fig. 2). Interestingly, in a different blinking QD system (CdSe/CdS core/shell QDs), a dim (gray) intermediate intensity peak has been reported in addition to the off and on peaks (trimodal blinking) and attributed to weekly emitting trion states.[3,37]

Models of blinking described in the literature are based on either or both of two mechanisms: the charging mechanism and the fluctuation of nonradiative recombination channels.[5] The originally proposed charging model and many of its versions developed later to explain the power law distributions[2] predict only two intensity states. An essential aspect of the charging model is an efficient Auger mechanism which renders trion states dark. As an extension of this framework, multiply charged states were suggested in order to account for a dark-state quantum yield much lower than its biexcitonic counterpart.[29] Multiply charged states are also consistent with the distribution of lifetimes in the dark state[38] as well as the present findings on the distribution of dark intensity states. The wide distribution of bright intensity states reported in this paper could be due to an alternative mechanism of fluctuating non-radiative channels. Surface trapping has been found to be an efficient non-radiative channel that can compete with radiative relaxation.[40] One might envision surface traps that are dynamically created and destroyed as a result of the relaxation processes of excited species. The resulting combination of a multiple charging mechanism and such fluctuating channels would explain these and possibly other important features of QD blinking. Note that the mechanism proposed to explain the blinking kinetics in the tertiary CdSe/CdS systems is an example of such a mixed mechanism: the off peak was due to efficient non-radiative channels and the dim (or gray) state was due to charging.[41]

An alternative theory is the multiple recombination center (MRC) model,[17] which attributes the intensity fluctuation to a dynamical set of recombination centers acting as two-level systems. These centers are thought to be dynamic trap states associated with the QD surface. A few such centers naturally produce a quasi-continuum of intensity states. Within this framework a separate dark and bright intensity state distribution is not due to charging, rather it can be achieved by assuming a strong interaction between the two-level systems.[17,42] Simulations using the interacting MRC model reveal in Fig. 5 that as the interaction strength is increased the bright and dark distributions become grouped into increasingly distinct and eventually non-overlapping manifolds. The interaction strength is quantified by the coupling parameter α. While at $\alpha = 0.3$ the two quantum yield distributions significantly overlap, at $\alpha = 0.9$ there is a large

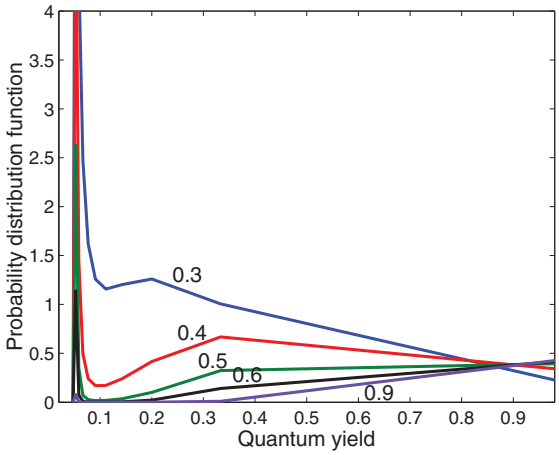

FIG. 5. Simulation of quantum yield (∼intensity) distribution function within the framework of interacting recombination centers. The lines (in order blue, red, green, black, and purple) correspond to an increasing coupling parameter α (0.3, 0.4, 0.5, 0.6, and 0.9). Other model parameters are kept constant.

gap in between the bright and dark groups. Meanwhile, the rest of the MRC parameters have been kept constant, and are similar to the ones used in previous calculations,[31] $N = 10$, $k_r/k = 0.5$, $\gamma_1 = 1$, $a = 1/\sqrt{10}$, and $\beta = -0.1$. Clearly, the extent of separation between the bright and dark groups is controlled by the coupling parameter. Note that the relative contribution of the two groups is controlled by the bias parameter β.

Even a qualitative comparison of the intensity distribution (Fig. 2) with simulated quantum yield distributions (Fig. 5) places constraints on the model parameters. Such a comparison is possible since, assuming constant excitation rate, the quantum yield is proportional with the intensity. It was argued earlier in this paper that the plateau in the experimental histogram corresponds to a gap in the underlying intensity distribution. Accordingly, the region roughly between 200 and 600 counts/ms in Fig. 4 (which is about 1/6–1/2 in quantum yield) is devoid of intensity states. This is a relatively large gap that can be rationalized within the MRC framework as a large coupling ($\alpha \approx 0.8$–0.9). Further theoretical investigation to uncover the microscopic nature of the two-level systems should reveal the reason for this constraint on the coupling parameter. Note, however, that since the extent of the flat feature is subject to binning artifacts the estimation of the coupling parameter based on the histogram plateaus is approximate. A variation in the apparent gap size of different trajectories is also noticeable, which at least partly, may be due to binning artifacts. It is possible to envision an approach which could provide more accurate estimations for the coupling parameter and indeed the full set of model parameters. This approach would be a direct Bayesian fit between the MRC model and a complete photon counting series, rather than a comparison via extracted statistics like the histogram and on/off distributions. Note that using photon counting series would eliminate binning and related artifacts altogether.

A framework providing a unified description was achieved recently by relaxing some of the assumptions of the originally proposed MRC model,[6] such as allowing for a special highly efficient recombination center. Further investigations revealed that such a unified framework seems to be consistent with the intensity distributions from all of the 100 trajectories analyzed here, including even those few with complicated distribution and multiple peaks in the histogram. Finally, an important realization should be mentioned, namely, that trap states are a common feature of both mechanisms of blinking. This suggests that future efforts should be aimed at understanding their microscopic nature.

A further implication of the Poisson fluctuations and blinking dynamics revealed hereby is that on and off statistics subtracted from trajectories by the threshold method could be strongly biased. While a large deviation from the average has a low relative probability, during very long on and off states this probability becomes significant resulting in events that effectively truncate and distort the distributions. Moreover, such effects would change as a function of the intensity threshold and bin time, resulting in an artificial dependence on these parameters. These observations support the conclusion of Crouch *et al.* that care must be taken when estimating statistics from trajectories.[14] Indeed, threshold and bin time dependence of the on and off statistics are routinely observed during trajectory analysis.[14,17] The single photon counting approach could be further developed to elucidate rigorously to what extent these dependencies are artifacts as opposed to being intrinsic to the underlying physical process. The present findings on the intensity histogram suggest that within the plateau region any threshold dependence should be purely artificial, whereas in the regions of the wider-than-Poissonian peaks would result as a combination of artifacts and the presence of the distributed intensity states. It is thus also of interest to investigate on methods to estimate unbiased statistics from binned trajectories.

V. CONCLUSIONS AND OUTLOOK

This study demonstrated a generic theoretical method for the treatment of binned photon counting statistics in single fluorophore blinking, and showed that one can learn valuable information about the number and nature of the underlying intensity states by its application in the analysis of the intensity histogram. The theoretical approach assumed a two-state system with known totally monotone WTDs of otherwise arbitrary functional form, which is one of its principal strengths. A specially tailored kinetic scheme of bright and dark nodes allowed for the control of the WTDs by varying the number and transition rate of the nodes. This was possible since the WTDs could be written as weighted sums of decaying exponentials each associated with a node. The method was applied on CdSe/ZnS core/shell QDs with power law WTDs, by comparing theoretical and experimental intensity histograms. A simple and efficient method was devised to test the two-state hypothesis on a large number of trajectories based on the contribution of dark peak probabilities.

From the comparison it became apparent that, in terms of qualitative features, histograms from telegraph-like quantum dot trajectories seem to roughly follow the two-state description. In particular, the two dominant bright and dark peaks and

the inter-peak plateaus were qualitatively reproduced. The shape, curvature, and especially tilt of the inter-peak features were found to be sensitive to the power law exponents. The analysis in this paper revealed a quasi-continuous distribution of bright and dark states grouped around two maxima. Overall, the presence of more-or-less flat plateaus indicates that these groups are separated by a gap of intensity states. This idea of a multi-state blinking, suggested by several earlier studies, is further supported in this work by a quantitative investigation involving a large number of trajectories compared to calculations with a wide range of parameters.

The present findings have implications on future microscopic models of blinking. On the one hand, a distribution of dark and bright states can be reconciled with a combination of multiple charging and trap-assisted dynamical non-radiative channels could probably reproduce these distributions. On the other hand, the multiple recombination center model,[17] can naturally explain such a quasi-continuum of states. The observation of the intensity state gap corresponding to the plateau feature in the intensity histogram indicates that the two-level systems used to model the recombination centers should be strongly interacting. Since both of these models of blinking assume dynamical trapping centers, one is led to the conclusion that the microscopic mechanism of blinking could be understood by uncovering the nature of the recombination centers. Here, a step has been taken towards this goal by providing constraints on the interaction parameter of the two-level systems used to model these centers at a phenomenological level. Since the MRC model can reproduce with ease various features of blinking, further investigation is warranted along its phenomenology. It is of interest to develop a Bayesian statistical method to give an accurate estimation of the parameters of recombination centers (their number, trapping rates, interaction, and bias parameters) from complete photon counting series.

Photon counting theory has been successfully applied to estimate fast protein folding rate assuming simple exponential kinetics.[43] According to our calculations $P(m|T)$ is quite sensitive to the change of the shortest timescales (Fig. 7), therefore it is of interest to further extend the treatment to the estimation of this timescale by comparison based on histograms. Another extension of the present photon counting method could be to calculate on and off time distributions known to exhibit strong threshold dependence,[17] as observed from binned trajectories. In particular, one ought to investigate the extent to which the choice of threshold can result in artificially biased on and off power law exponents, as well as to estimate their true values. Note that such calculations would be especially useful for fluorophores that can be described as true or approximate two-level systems. During the review process of the present paper a study was published along these lines using simulated trajectories with power law waiting times.[44]

ACKNOWLEDGMENTS

The author would like to thank Dr. R. A. Marcus, Dr. B. Jankó, Dr. P. A. Frantsuzov, Dr. A. Szabo, and Dr. M. Kuno for fruitful discussions and valuable advice. Support by grants from the James W. Glanville Foundation at the California Institute of Technology, the Office of Naval Research, and the Army Research Office are gratefully acknowledged. The author feels indebted to Dr. M. Kuno for sharing a large number of trajectories.

APPENDIX A: THE NUMERICAL COMPUTATION OF F'_m

The most general case is considered where the order of approximation in Eq. (21) is arbitrary. Calculations are formally much simplified if a tensor algebra is employed. Tensors are built up from vectors of dimensions N_b and N_d after a repeated application of the outer product operation. For example, a 2-dimensional tensor result from the outer product of two vectors, $\overleftrightarrow{T} = \vec{u} \otimes \vec{v}$, using the definition

$$(\vec{u} \otimes \vec{v})_{ij} = u_i u_j. \tag{A1}$$

This definition is then generalized to tensors of arbitrary dimensions. The dot product must be also defined,

$$(\overleftrightarrow{A} \cdot \overleftrightarrow{B}) = \sum_{i,j,\ldots} A_{ij\ldots} B_{ij\ldots}. \tag{A2}$$

As a benefit of the tensor notation one can separate the λ and s dependent part from a constant in Eq. (24). By employing the properties from Eqs. (22) and (23) F'_m can be recast as

$$\begin{aligned}
&F'_m(l_1, l_2, l_3, l_4) \\
&= (-1)^m \\
&\quad \times \overleftrightarrow{K} \cdot \mathcal{L}^{-1} \left\{ \frac{d^m}{ds^m} \underbrace{\left(\frac{1}{s+\vec{H}^b} \otimes \cdots \otimes \frac{1}{s+\vec{H}^b} \right)}_{l_1+l_3=L^b \text{ terms}} \underbrace{\otimes \frac{1}{s+\vec{H}^d} \cdots}_{l_2+l_4=L^d \text{ terms}} \right. \\
&\quad \cdots \\
&\quad + r^n C_n^{m-n} \frac{d^{m-n}}{ds^{m-n}} \left(\frac{1}{s+\vec{H}^b} \otimes \cdots \right) \frac{d^n}{ds^n} \left(\otimes \frac{1}{s+\vec{H}^d} \cdots \right) \\
&\quad \cdots \\
&\quad \left. + r^m \left(\frac{1}{s+\vec{H}^b} \otimes \cdots \right) \frac{d^m}{ds^m} \left(\otimes \frac{1}{s+\vec{H}^d} \cdots \right) \right\},
\end{aligned}$$

where $\vec{H}_b = \vec{1} + \vec{K}_b$ and $\vec{H}_d = r\vec{1} + \vec{K}_d$, while $C_n^{m-n} = (m-n)!/(m!n!)$, $n = \{0, \ldots, m\}$ is the number of combinations for a subset of n elements chosen from a set of $(m-n)$ elements. The constant tensor is defined as $\overleftrightarrow{K} = (\vec{K}_b \otimes)^{l_1} (\vec{1} \otimes)^{l_3} (\vec{K}_d \otimes)^{l_2} (\vec{1} \otimes)^{l_4} 1$. By using the convolution theorem and standard formulas for derivatives of the Laplace-transform Eq. (A3) is effectively reduced to inverting the two tensors in brackets of dimensions L_b and L_d, respectively,

$$\begin{aligned}
&F'_{m,T}(l_1, l_2, l_3, l_4) \\
&\quad = \overleftrightarrow{K} \cdot \sum_{n=0}^{m} r^n C_n^{m-n} \\
&\qquad \times \int_0^T [t^{m-n} \mathcal{L}^{-1}\{(s+\vec{H}^b)^{-1} \otimes \cdots\}(t) \\
&\qquad \times (T-t)^n \mathcal{L}^{-1}\{\otimes (s+\vec{H}^d)^{-1} \cdots\}(T-t)] dt.
\end{aligned}$$

The Laplace-inversions and integration in Eq. (A3) can be carried out computationally by symbolic calculation for a very limited number of nodes. However, this *direct method* quickly becomes computationally unfeasible as the number of nodes is increased, e.g., to yield smooth weighting distributions spanning perhaps orders of magnitude in this time.

One can tackle this challenge by introducing small variations $\delta\vec{H}^b$ and $\delta\vec{H}^b$ in $\vec{H}^b$ and $\vec{H}^d$. The goal of this "variational method" is to prevent any identical elements in the expressions to be Laplace-inverted in Eq. (A3). This mathematical device allows for a unified analytical formula for the Laplace inversions. For a general treatment let us assign index j to vectors $\vec{H}$ noting that $\vec{H}^j$ can be either $\vec{H}^b$ or $\vec{H}^d$,

$$\begin{aligned}&\mathcal{L}^{-1}\left\{\left(s+H_{l_1}^1\right)^{-1}\left(s+H_{l_2}^2\right)^{-1}\dots\right\}(t)\\&\quad\to\mathcal{L}^{-1}\left\{\left(s+H_{l_1}^1+\delta H_{l_1}^1\right)^{-1}\left(s+H_{l_2}^2+\delta H_{l_2}^2\right)^{-1}\dots\right\}(t)\\&\quad=\sum_j e^{-(H_{l_j}^j+\delta H_{l_j}^j)t}\prod_{j'\neq j}\frac{1}{\left(H_{l_{j'}}^{j'}+\delta H_{l_{j'}}^{j'}\right)-\left(H_{l_j}^j+\delta H_{l_j}^j\right)},\end{aligned}\tag{A3}$$

since $H_{l_j}^j+\delta H_{l_j}^j\neq H_{l_{j'}}^{j'}+\delta H_{l_{j'}}^{j'}$ for any $j\neq j'$ even if $H_{l_j}^j=H_{l_{j'}}^{j'}$ since no two variations are allowed to be identical. The variations are random numbers which are gradually reduced until sufficient convergence is achieved.

In Eq. (A3), the time dependence enters only through exponentials. Therefore, introducing the notations $\alpha_l=H_l+\delta H_l$ and $\beta_{l'}=H'_{l'}+\delta H'_{l'}$ the time-dependent part of the elements of the convolution integral tensor in Eq. (A3) can be recast as

$$\begin{aligned}&\int_0^T t^{m-n}e^{-(H_l+\delta H_l)t}(T-t)^n e^{-(H'_{l'}+\delta H'_{l'})(T-t)}\,dt\\&\quad=\frac{e^{-\alpha_l T}T^{m+1}}{(m+1)!}\,{}_1F_1(n+1,m+2,(\alpha_l-\beta_{l'})T).\end{aligned}\tag{A4}$$

Since in practical applications the number of photons per bin is often in the hundreds care must be taken in avoiding variable over- and underflow due to the factorial term in Eq. (A4).

Both the direct and variational methods have been implemented using the powerful symbolic and array (tensor) tools of MATLAB.[45] With the purpose of validation test computations have been performed to compare the variational result to the corresponding exact result.

APPENDIX B: EXPONENTIAL WTDs: VALIDATION OF TECHNIQUE

Here, the simplest case is considered, whereby both bright and dark WTDs are simple exponential functions. This is equivalent to having only one node for each of the two intensity states, i.e., $N_b=N_d=1$. This particular case was already treated by Gopich and Szabo, who have given an analytic formula for the probabilities $P(m|T)$.[16] Their results are accurately reproduced in Fig. 6 as a means of verifying the correctness of the present technique. Note that as opposed to the calculations of Gopich and Szabo, the present method involved several reasonable approximations that made calculations tractable. The perfect agreement between the two calculations indeed validates these approximations.

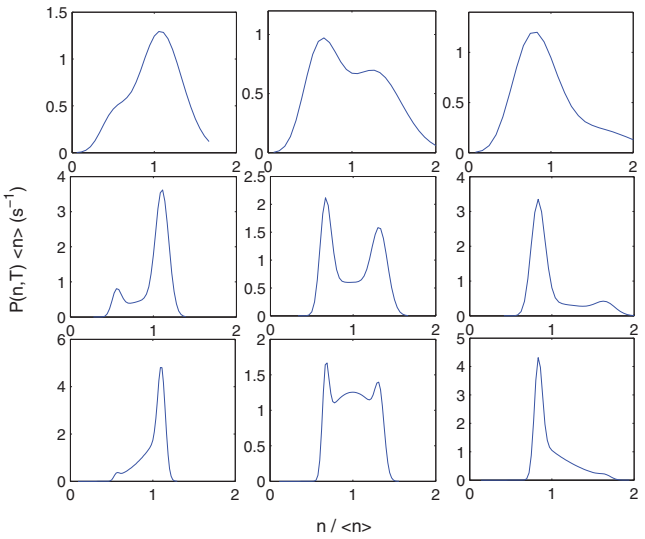

FIG. 6. The distribution of the number of turnovers in a bin for exponential WTDs calculated for a series of bin times and bright ↔ dark switching rates. The dark state is only "dim" since its emission rate is only $r=1/2$ of the bright intensity: $n_d=1\,\mathrm{ms}^{-1}$ and $n_b=2\,\mathrm{ms}^{-1}$. The rows correspond to bin times of 10 ms (top row), 100 ms (middle row), and 300 ms (bottom row). The columns correspond to different bright and dark switching rates, namely, $K_b=8\,\mathrm{s}^{-1}$ and $K_d=2\,\mathrm{s}^{-1}$ (left column), $K_b=K_d=5\,\mathrm{s}^{-1}$ (center column), and finally $K_b=2\,\mathrm{s}^{-1}$ and $K_d=8\,\mathrm{s}^{-1}$ (right column).

Another validity test, a simple one, is that $P(m|T)$ being a well-defined probability should yield 1 after summation over m. This normalization test can be always performed irrespective of the functional form of the WTDs. These include such relevant functions as power laws and stretched exponentials, for which, to my best knowledge, no calculations have been reported in literature before this study.

It is expected that as bin times are increased a central peak shows up in addition to the two Poissonian-like peaks corresponding to the dark (dim) and bright states. This effect is due to the fast transitions between the two states when compared to bin time. The central peak is quite evident for the $K_b=K_d$ case (Fig. 6 bottom line, center column), whereas for more eccentric bright/dark peak ratios a flat inter-peak feature is seen. For long enough bin times the central peak is expected to dominate regardless of the parameters in the kinetic scheme.

APPENDIX C: STATISTICAL CONFIDENCE INTERVAL ESTIMATION FROM TRAJECTORIES

This section describes the details of the method for confidence interval estimation for the off peak probability contributions and mean quantum yield from trajectory histograms. The f_n notation will be used for the number of intensity points corresponding to the count n.

The off (dark) peak of dichotomous-like (two-peak in the histogram) trajectories is typically narrow and can be fitted well by a Poissonian centered at 2–3 bin units in the histogram. Due to blinking dynamics, the inner (right side) base

of the peaks becomes much wider and thus the Poissonian fit is usually limited to about 3–5 bin units in the histogram. The estimation method proceeds in two steps. First, a maximum likelihood method is used assuming a Poissonian $P_n(\lambda)$ distribution of these first n_0. Here, λ corresponds to the maximum of the Poisson peak, i.e., the background photon count level. One has to search for the maximum of the log-likelihood function

$$L(\lambda) = -N_d\lambda + \log(\lambda)\sum_n (nf_n) - \sum_n f_n \log(n!) - N_d \log\left(\sum_n P_n(\lambda)\right), \quad \text{(C1)}$$

where $N_d = \sum_n f_n$ and summations run from $n = 0$ to $n = n_d$. Due to the large number of data points in these first bins (of the order of 1000), one can assume a Gaussian distribution around the maximum likelihood at λ_0 which yields the standard deviation (STD) $\sigma_{\lambda 0}$.

In the second step, one can estimate the probability contribution of the dark peak, to which a stochastic variable a will be assigned. Using the notation $N = \sum_{n=0}^{\infty} f_n$ the variable

$$a_n = \frac{f_n}{N P(n, \lambda)} \quad \text{(C2)}$$

will be defined, which is the estimation for a using only one histogram point, f_n. Since the f_n are assumed to be Poisson-distributed with STD $(NaP_n(\lambda))^{1/2}$, and they are large numbers, the standard variable $b_n = (a - a_n)(NP_n(\lambda)/a)^{1/2}$ is very well approximated by a Gaussian centered at 0 and having STD of 1, $G(0, 1)$. From here follows that $\sum_{n=0}^{n_d} b_n$ is distributed as $G(0, 1/\sqrt{n_d + 1})$, which is a function of a. The pair distribution function (PDF) of a follows by a change of variables from $\sum_{n=0}^{n_d} b_n \to a$. Note that this is a conditional PDF since a_n is a function of λ, prob$(a|\lambda)$. Due to the large number of data points it is safe to assume that the distribution of λ given by the likelihood method is independent of the distribution of a_n, therefore the probability associated with a is

$$\text{prob}(a) = \int \text{prob}(a|\lambda)\text{prob}(\lambda)d\lambda. \quad \text{(C3)}$$

In order to find the confidence intervals one needs the cumulative probability, which involves integration with respect to a as well,

$$\text{prob}\{a < a_1\} = \int_0^{a_1} da \int_0^{\infty} d\lambda \frac{1}{4\pi\sigma_{\lambda 0}} \times \exp\left[-N(a - a_\lambda)^2 \frac{P_n(\lambda)}{2a}\right] \times \exp\left[-\frac{(\lambda - \lambda_0)^2}{2\sigma_{\lambda 0}^2}\right] J(a, \lambda), \quad \text{(C4)}$$

where the Jacobian is due to the change of variables,

$$J(a, \lambda) = \frac{1}{2n_d\sqrt{a}}\left[\frac{1}{a\sqrt{N}}\sum_n \frac{f_n}{\sqrt{P_n(\lambda)}} + \sqrt{N}\sum_n \sqrt{P_n(\lambda)}\right]. \quad \text{(C5)}$$

A 95% confidence region corresponding to the interval (a_1, a_2) can be found by solving the integration assuming the relations prob$\{a < a_1\} = 2.5\%$ and prob$\{a < a_2\} = 97.5\%$.

The estimation of the mean quantum yield confidence intervals involves finding the 100% quantum yield bright emission rate. The on peak is too wide for a Poissonian fit; therefore, a less rigorous method is used. One can assume a very broad region starting at the maximum of the on peak and extending almost to the end of the on tail. This choice makes it practically certain that this region will contain the 100% quantum yield state.

APPENDIX D: SHORTEST TIMESCALES FOR POWER LAW WTDs

The effect of the shortest timescale ($t_m^{b(d)}$) on the flat conformational dynamics feature (Fig. 7) is investigated. For simplicity, identical shortest times were chosen for both bright and dark WTDs, and calculations were performed by varying them over a range spanning one order of magnitude, from 5 ms to 50 ms. In qualitative agreement with basic observations on QD fluorescence intermittency, a 10:1 ratio between the longest timescales is assumed in favor of the dark

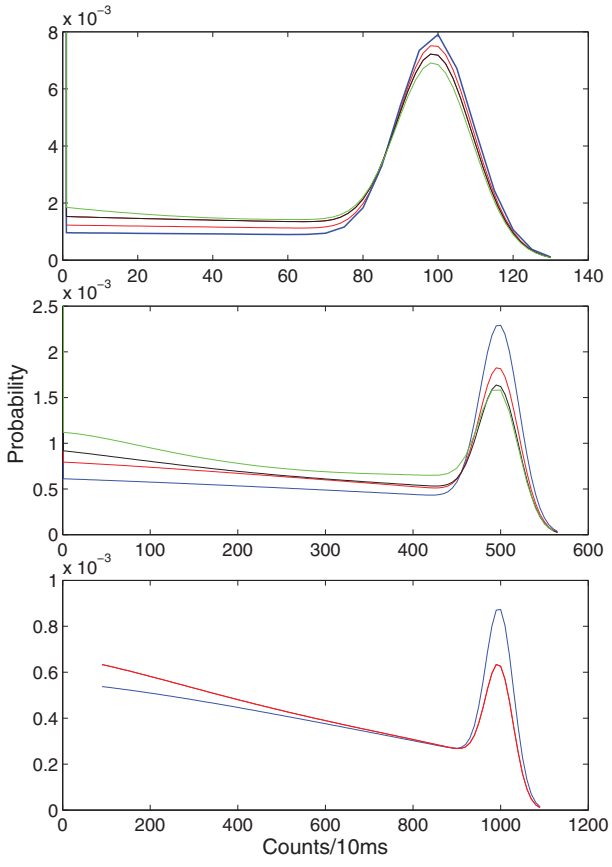

FIG. 7. The probability of counts in a bin as a function of the shortest timescale of the WTDs. The figures show the effect for different bin sizes, 10 ms (a), 50 ms (b), and 0.1 s (c). Within each panel the plots correspond to shortest timescales of $t_m^{b(d)} = 50$ ms (blue), $t_m^{b(d)} = 20$ ms (red), $t_m^{b(d)} = 10$ ms (black), and $t_m^{b(d)} = 5$ ms (green), respectively. Longest timescales were $t_M^d = 1s$ and $t_M^b = 0.1$ s, throughout. Other parameters were $\alpha_{b(d)} = 1.5$ and $\langle Y \rangle = 0.1$.

intensity state, as well as a pronounced asymmetry between the probability of being in the dark versus bright states (9:1). The results in Fig. 7 show the expected effect upon changing the shortest timescale: the shorter it is, the more pronounced the inter-peak flat feature becomes. In the meantime, a consistent shrinking of the bright peak is observed. While the relative size of the features is affected, the overall picture does not change qualitatively over the range of 5 ms–50 ms.

[1]F. Cichos, C. von Borczyskowski, and M. Orrit, Curr. Opin. Colloid Interface Sci. **12**, 272 (2007).
[2]P. A. Frantsuzov, M. Kuno, B. Jankó, and R. A. Marcus, Nat. Phys. **4**, 519 (2008).
[3]W. Qin and P. Guyot-Sionnest, ACS Nano **6**, 9125 (2012).
[4]M. Kuno, D. P. Fromm, H. F. Hammann, A. Gallagher, and D. J. Nesbitt, J. Chem. Phys. **112**, 3117 (2000).
[5]A. A. Cordones and S. R. Leone, Chem. Soc. Rev. **42**, 3209 (2013).
[6]P. A. Frantsuzov, S. Volkán-Kacsó, and B. Jankó, Nano Lett. **13**, 402 (2013).
[7]L. K. Schirra, B. S. Tackett, M. L. Blumenfeld, and O. L. A. Monti, J. Chem. Phys. **131**, 124702 (2009).
[8]S. Unterkofler, T. Pflock, J. Southall, R. J. Cogdell, and J. Kohler, ChemPhysChem **12**, 711 (2011).
[9]K. P. Ghiggino, T. D. M. Bell, and E. N. Hooley, Faraday Discuss. **155**, 79 (2012).
[10]C. Bradac, T. Gaebel, N. Naidoo, M. J. Sellars, J. Twamley, L. J. Brown, A. S. Barnard, T. Plakhotnik, A. V. Zvyagin, and J. R. Rabeau, Nat. Nanotechnol. **5**, 345 (2010).
[11]A. L. Efros and M. Rosen, Phys. Rev. Lett. **78**, 1110 (1997).
[12]G. Margolin and E. Barkai, J. Chem. Phys. **121**, 1566 (2004).
[13]K. Zhang, H. Chang, A. Fu, A. P. Alivisatos, and H. Yang, Nano Lett. **6**, 843 (2006).
[14]C. H. Crouch, O. Sauter, X. Wu, R. Purcell, C. Querner, M. Drndic, and M. Pelton, Nano Lett. **10**, 1692 (2010).
[15]I. Gopich and A. Szabo, *Theory and Evaluation of Single-Molecule Signals* (World Scientific Publishing, 2008).
[16]I. Gopich and A. Szabo, J. Chem. Phys. **124**, 154712 (2006).
[17]P. A. Frantsuzov, S. Volkán-Kacsó, and B. Jankó, Phys. Rev. Lett. **103**, 207402 (2009).
[18]S. Bernstein, Acta Math. **52**, 1 (1929).
[19]G. Beylkin and L. Monzón, Appl. Comput. Harmon. Anal. **19**, 17 (2005).
[20]I. Gopich and A. Szabo, J. Chem. Phys. **118**, 454 (2003).
[21]F. L. H. Brown, Phys. Rev. Lett. **90**, 028302 (2003).
[22]J. Sherman and W. J. Morrison, Ann. Math. Stat. **21**, 124 (1950).
[23]M. R. Spiegel, *Schaum's Outline of Mathematical Handbook of Formulas and Tables* (Schaum Publishing Co., 1968).
[24]M. Blum, Proc. IEEE **52**, 308 (1964).
[25]E. W. Barnes, Proc. London Math. Soc. **s2-5**, 59 (1907).
[26]M. Abramovitz and I. A. Stegun, *Handbook of Mathematical Functions*, 10th ed. (National Bureau of Standards, Department of Commerce, USA, 1972).
[27]J. P. Hoogenboom, J. Hernando, E. M. H. P. van Dijk, N. F. van Hulst, and M. F. Garsia-Parajo, ChemPhysChem **8**, 823 (2007).
[28]G. Margolin, V. Protasenko, M. Kuno, and E. Barkai, J. Phys. Chem. B **110**, 19053 (2006).
[29]J. Zhao, G. Nair, B. R. Fisher, and M. G. Bawendi, Phys. Rev. Lett. **104**, 157403 (2010).
[30]F. D. Stefani, X. Zhong, W. Knoll, M. Han, and M. Kreiter, New J. Phys. **7**, 197 (2005).
[31]H. Steinberg, O. Wolf, A. Faust, A. Salant, Y. Lilach, O. Millo, and U. Banin, Nano Lett. **10**, 2416 (2010).
[32]G. Schlegel, J. Bohnenberger, I. Potapova, and A. Mews, Phys. Rev. Lett. **88**, 137401 (2002).
[33]C. Santori, D. Fattal, J. Vučković, G. S. Solomon, E. Waks, and Y. Yamamoto, Phys. Rev. B **69**, 205324 (2004).
[34]J. Lamperti, Trans. Am. Math. Soc. **88**, 380 (1958).
[35]G. Margolin and E. Barkai, Phys. Rev. Lett. **94**, 080601 (2005).
[36]K. T. Shimizu, R. G. Neuhauser, C. A. Leatherdale, S. A. Empedocles, W. K. Woo, and M. G. Bawendi, Phys. Rev. B **63**, 205316 (2001).
[37]D. E. Gomez, J. van Embden, P. Mulvaney, M. J. Fernee, and H. Rubinsztein-Dunlop, ACS Nano **3**, 2281 (2009).
[38]S. Rosen, O. Schwartz, and D. Oron, Phys. Rev. Lett. **104**, 157404 (2010).
[39]A. A. Cordones, T. J. Bixby, and S. R. Leone, Nano Lett. **11**, 3366 (2011).
[40]P. Tyagi and P. Kambhampati, J. Chem. Phys. **134**, 094706 (2011).
[41]A. K. Gooding, D. E. Gómez, and P. Mulvaney, ACS Nano **2**, 669 (2008).
[42]S. Bianco, E. Geneston, P. Grigolini, and M. Ignaccolo, Physica A **387**, 1387 (2008).
[43]H. S. Chung, I. V. Gopich, K. McHale, T. Cellmer, J. M. Louis, and W. A. Eaton, J. Phys. Chem. A **115**, 3642 (2011).
[44]N. Amecke, A. Heber, and F. Cichos, J. Chem. Phys. **140**, 114306 (2014).
[45]*MATLAB. The Language of Technical Computing* (MathWork, Inc., 1984–2008, Version R2008b).